



# Effect of welding parameters on microstructure and mechanical properties of mild steel components produced by WAAM

Nataliia Chernovol<sup>1</sup> · Fereidoon Marefat<sup>2</sup> · Bert Lauwers<sup>1</sup> · Patrick Van Rymenant<sup>1</sup>

Received: 28 July 2022 / Accepted: 18 November 2022 / Published online: 29 November 2022  
© International Institute of Welding 2022

## Abstract

The GMAW-based wire and arc additive manufacturing is widely used for cost- and material-efficient production of medium to large metal parts. Nevertheless, the application of metal parts produced by WAAM depends on their mechanical properties. This paper investigates the impact of welding heat input (HI) on the microstructure and mechanical properties of solid WAAM parts. For this purpose, three blocks were deposited from low-carbon low-alloy steel with various welding parameters in a multi-pass multilayer way. The microstructure of the solid WAAM parts consists of the repetitive pattern of the primary constituent, which contains columnar, fine grain, and coarse grain zones. Changes in microstructure provoked by an increase in HI were correlated with hardness in each zone of the primary constituent, tensile, and impact toughness properties of the material. It was revealed that the increase in HI leads to the reduction of material hardness, yield, and ultimate tensile strength. At the same time, the percentage elongation after fracture and impact toughness of the material improve with the rise of HI. The anisotropy of the material was analysed based on the mechanical properties in longitudinal, vertical, and transversal directions. For filler wire selection, the properties of the WAAM material were compared to the properties specified in the wire certificate and the corresponding standard for welding wire, as well as to the properties of hot-rolled structural steels. The results showed that the G 42 4 M21 3Si1 (EN ISO 14341-A) wire is suitable to produce functional components using WAAM as an alternative for conventional subtractive manufacturing of parts from S275JR and S355JR structural steels taking static loads and impact loads.

**Keywords** Gas metal arc welding · Additive manufacturing · Mild steel · Mechanical properties · Microstructure characterization

## 1 Introduction

Nowadays, metal additive manufacturing (AM) techniques are widely used for rapid prototyping and production of workpieces in small batches. Compared to the conventional production processes, it allows to reduce the lead time, amount of scrap material, and cost of the part [1, 2]. Additionally, AM provides flexibility to produce multi-material

parts and parts with complex geometries. One of the AM techniques for manufacturing medium to large size metal parts with medium geometrical complexity is wire and arc additive manufacturing (WAAM). WAAM uses an electric arc as a heat source to melt a filler wire and build a component in a layer-by-layer manner.

There are three welding technologies used for WAAM: gas metal arc welding (GMAW), gas tungsten arc welding (GTAW), and plasma arc welding (PAW). GMAW is the most widely used technique for WAAM due to its high deposition rates (1 to 4 kg/h [3]), the possibility to deposit a wide range of materials, simplified programming of the motion system as the filler wire is coaxial with the nozzle, and lower cost of the equipment. Nevertheless, one of the main barriers to technology integration in the industry is the safe application of the WAAM parts, which highly depends on their mechanical properties. Materials such as Ti-6Al-4 V [4, 5], stainless steel [6], aluminium alloys [7], and Ni superalloys

---

Recommended for publication by Commission I—Additive Manufacturing, Surfacing, and Thermal Cutting.

✉ Nataliia Chernovol  
nataliia.chernovol@kuleuven.be

<sup>1</sup> Department of Mechanical Engineering, KU Leuven, Celestijnenlaan 300, Leuven 3001, Belgium

<sup>2</sup> Department of Materials Engineering, KU Leuven, Kasteelpark Arenberg 44, Leuven 3001, Belgium

have been widely investigated. Even though structural steels were also explored, there is a limited number of studies devoted to the effect of welding parameters on the mechanical properties of WAAM produced mild steels.

Various microstructural constituents are formed in a mild and low-alloyed low-carbon weld metal. Commonly found constituents are grain boundary ferrite, polygonal ferrite, pearlite, bainite, acicular ferrite, and martensite/austenite (M/A) [8]. The volume fraction of the microstructural constituents depends on the reheating and cooling cycles [8]. Several studies were devoted to the determination of the microstructure and mechanical properties of thin-walled WAAM parts, deposited in a single-pass multilayer manner. Depending on the microstructure, three main zones were identified for all the samples: lower zone near the substrate plate, middle zone, and upper zone — last pass(es). The lower zone is characterized by a fine-grained mixed microstructure, and thus higher microhardness values, due to the shorter cooling times (i.e., cooling time from 800 to 500 °C —  $t_{8/5}$  according to EN 1011–2) caused by the lower values of the initial temperatures and better heat dissipation conditions. With the increase in the number of layers, temperature accumulates (due to the decrease in conduction and higher values of the initial temperatures) leading to slower cooling (longer  $t_{8/5}$  cooling time). The middle zone is characterized by the pattern of coarse-grained and fine-grained heat-affected zone (HAZ) [9]. As a result, the lowest microhardness values are observed there. The upper zone does not experience reheating and is characterized by a fine-grained microstructure and higher hardness values.

Some studies were done to determine the influence of the welding heat input (HI) on the mechanical properties of thin-walled WAAM parts produced in a single-pass multilayer manner. It was concluded that HI has no impact on the mechanical properties of low-alloy and high-strength low-carbon WAAM parts as the cooling curves and peak temperatures are almost the same for all the samples [10, 11].

The isotropy of the mechanical properties and homogeneity of the obtained microstructure have also been investigated. Some researchers report about the isotropic properties, others about the significant dependency of the properties on the test direction (for instance, along the deposition direction and along the build direction). As such, Haden et al. [12] compared the tensile properties of thin-walled WAAM parts produced from mild steel and concluded that there is no significant difference in yield strength between the horizontal and vertical directions. At the same time, ultimate tensile strength (UTS) is direction-dependent. In contrast, Lu et al. [13] reported a significant difference in yield strength (YS), UTS, and elongation between the horizontal and vertical samples. They concluded that the mechanical properties of the thin-walled WAAM components are anisotropic. Waqas et al. [14] studied the dependency of the

test direction on fracture toughness of single-pass multilayer WAAM walls and concluded that there is no significant difference in impact toughness between the vertical and horizontal samples.

In the case of multi-pass multilayer deposition, the temperature of the substrate continuously increases. Also, during production, heat dissipation conditions are changing. As a result, cooling rates will differ for the different passes and layers. Moreover, the bead of a specific pass will also be partially re-melted and further tempered by the adjacent passes within one layer and by passes of the next layers. The final microstructure depends on the peak temperatures and heating and cooling rates. The main factors influencing heating and cooling rates during WAAM are interpass temperature (or interpass idle time), interlayer temperature (or interlayer idle time), heat input, and deposition path strategy.

Shassere et al. [9] reported the stable and isotropic mechanical properties of WAAM walls deposited in two passes multilayer way during metal big area additive manufacturing (MBAAM). Closed-loop correction control that actively adjusts the wire feed speed during the surface tension transfer process leads to polygonal ferrite and pearlite formation in most of the build combined with uniform hardness properties. Nevertheless, scatter was observed in the properties of the last bead and a region near the substrate plate.

The influence of deposition path strategy on the mechanical properties and microstructure of the final component has been investigated only for raster and zig-zag patterns. Sridharan et al. [15] investigated toughness scatter in low-carbon C-Mn steel. A significant variation in tensile ductility and Charpy toughness was observed depending on the building direction. Microstructural heterogeneity was observed as well in all samples and is explained by variation in cooling rates and heat accumulation during the process. Zhang et al. [5] studied fracture and fatigue crack growth properties of Ti-6Al-4 V parts produced by WAAM depending on the wire composition, test direction, and deposition path strategy. They concluded that fracture toughness depends on the direction (i.e., across and along the deposition direction) and deposition strategy. It was observed that fracture toughness is higher for the oscillation strategy than for the parallel strategy. Fu et al. [16] investigated the influence of the lap way between layers and layers in the toolpath on the mechanical properties of Ti-6Al-4 V. A significant difference in tensile strength and strain of the samples was observed. Song et al. [17] determined the influence of the deposition path strategy on the mechanical properties of WAAM printed parts. Four deposition strategies were compared: unidirectional (one-way) with the alternate angle between the layers 0° and 90°, and zig-zag with the alternate angle between the layers 0° and 90° (Fig. 1). It was concluded that deposition direction between the layers has a significant effect on tensile

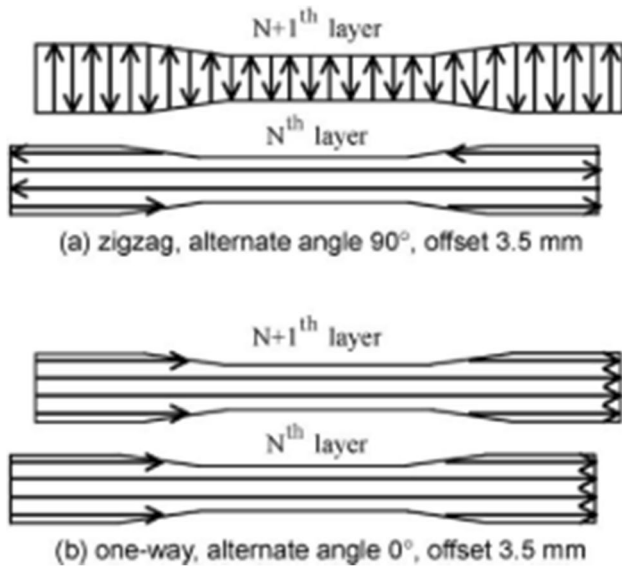


**Fig. 1** 3D welded and milled tensile test specimens and applied deposition strategies [17]

strength ( $P=97.717\%$ , ANOVA). Nevertheless, the effect of deposition direction within the layer is low ( $P=0.035\%$ , ANOVA).

To summarize, the mechanical properties of WAAM samples depend on many aspects related to the WAAM process parameters and conditions. Thus, based on the achieved material characteristics studied on simple WAAM walls and cubes, one cannot state that WAAM parts with other configurations will have similar properties. Recently, the American standard AWS D20.1/D20.1 M:2019 “Specification for Fabrication of Metal Components using Additive Manufacturing” has been developed. According to it, inspection and testing should be performed for the qualification of both machine and procedure. Under the machine and procedure changes, the following components are specified:

- Build design
- Material (i.e., wire diameter and composition and substrate plate)
- Machine (manufacturer, location, software, etc.)
- Environment (including interpass temperature, cooling or preheating of the substrate, and shielding gas)
- Heat source characteristics
- Deposition characteristics (i.e., travel speed of the robot (TS), wire feed speed (WFS), and step-over value)
- Post-build heat treatment/processing (includes post weld heat treatment (PWHT) and surface finish method, e.g., milling)

This paper is devoted to the determination of the impact of HI on the microstructure, mechanical properties, and

anisotropy of solid mild steel WAAM blocks. The obtained results are compared to both wrought material and filler wire properties. The comparison provides the necessary information to estimate the mechanical properties for future fabricated solid WAAM components.

## 2 Materials and methods

To analyse the impact of the WAAM parameters on the mechanical properties and microstructure, three solid blocks were deposited in a multi-pass multilayer way using different welding parameters. For each block, the following tests were implemented: (1) microstructure evaluation; (2) tensile test; (3) Charpy impact test; and (4) Vickers hardness measurement.

To study the impact of WAAM process parameters on the anisotropy of the material, samples were produced in three directions: vertical — along the build direction (Z-axis), longitudinal — along the weld direction (Y-axis), and transversal — direction perpendicular to longitudinal (X-axis). In each direction, samples with two orientations were analysed. The orientation of tensile specimens is shown in Fig. 2 (from left to right — vertical, transversal, and longitudinal samples).

For the Charpy impact test, the notch’s location and the test force’s direction define the direction and orientations of the samples. The schematic representation of specimens for Charpy impact toughness is shown in Fig. 3 (from left to right — vertical, transversal, and longitudinal samples).

Samples for tensile testing, Charpy impact testing, Vickers hardness measurement, and microstructure evaluation were fitted within the block. Dimensions of the deposited block are  $142.5 \times 75 \times 80 \text{ mm}^3$  (length  $\times$  width  $\times$  height). The design of the block is shown in Fig. 4.

A CLOOS QRC320H robot cell served as the motion system. Samples were deposited using a Qineo pulse 450A welding power source with synergic control in standard GMAW mode. The substrate plate was a mild steel plate with dimensions  $200 \times 250 \times 10 \text{ mm}^3$ . As filler material, a 1.2 mm diameter copper coated wire EN ISO 14341-A (G 42 4 M21 3Si1) was used (Table 1). The shielding gas was Ar with a 15%  $\text{CO}_2$  mixture at a constant flow rate of 15 l/min. Contact tip to work distance (CTWD) was kept constant during deposition at 15 mm. Blocks were deposited using zig-zag deposition strategy. The beads within one layer were deposited in one direction. The deposition direction of every second layer was reversed. Interpass time was equal to the welding time per pass. Additionally, interlayer cooling time equal to the total time for deposition of one layer was used to prevent significant temperature accumulation. The temperature between the layers

**Fig. 2** Schematic representation of tensile specimens positioned along 3 directions and having 2 orientations

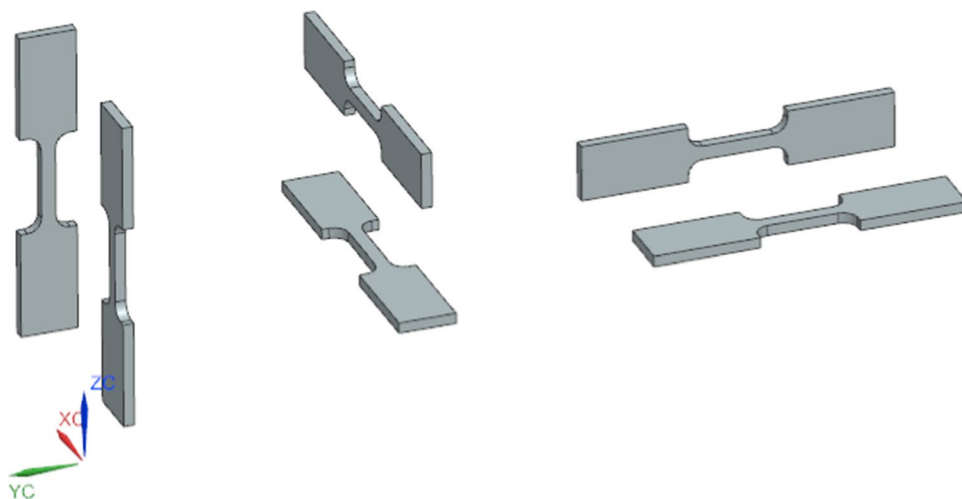
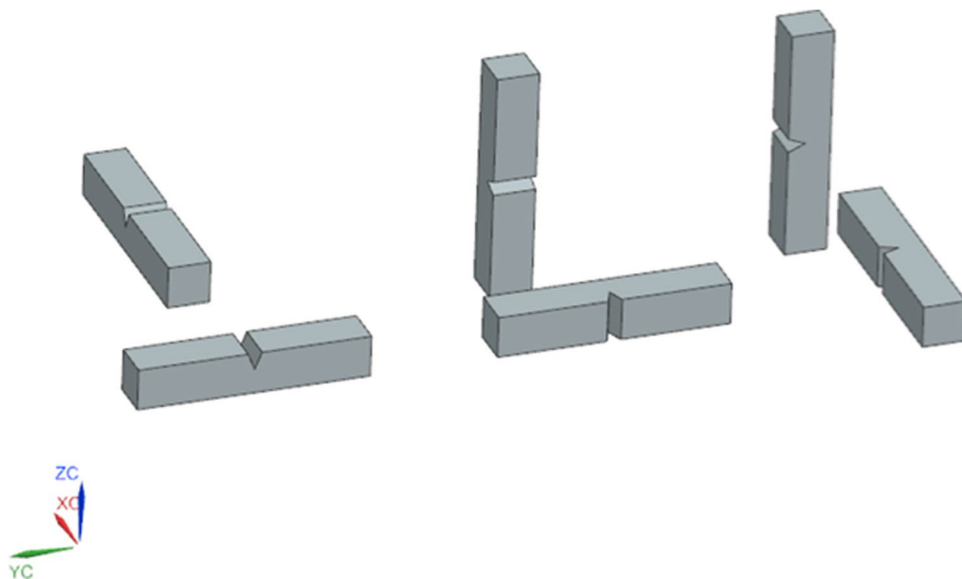


**Fig. 3** Schematic representation of specimens for Charpy impact toughness positioned along 3 directions and having 2 orientations



was controlled using temperature indicator crayons and did not exceed 250 °C. WAAM process parameters are provided in Table 2.

After deposition, samples were machined (milling) to remove the rough surface obtained after WAAM. Ultrasonic testing was implemented and detected multiple defects at varying depths in the block produced with the lowest HI. The presence of these defects can be explained by the unstable behaviour of the arc leading to the uneven beads overlapping (Fig. 5).

The deposition of two other blocks was stable, and only a few small imperfections were detected. Based on this, the mechanical properties were determined only for the two blocks deposited with average and high HI. For future parts, we would not recommend depositing solid components with the lowest HI values.

## 2.1 Microstructure characterization

After non-destructive testing (NDT), specimens for microstructural examination were made using wire EDM. For this study, the samples were selected from the centre of the blocks in horizontal and vertical directions as shown in Fig. 6. Samples were prepared by grinding and polishing with 3 µm diamond powder. Further, samples were etched with 2% Nital. Optical imaging was conducted using a HIROX digital microscope KH-8700.

## 2.2 Tensile testing

Currently, there is no standard available for tensile testing of components produced by WAAM. As an alternative, the ISO 6892-1:2009 standard for tensile testing of metallic

**Fig. 4** Specimens fitting within the block: (blue) — tensile specimens, (green) — Charpy specimens, (orange) — specimens for microstructure and Vickers hardness mapping

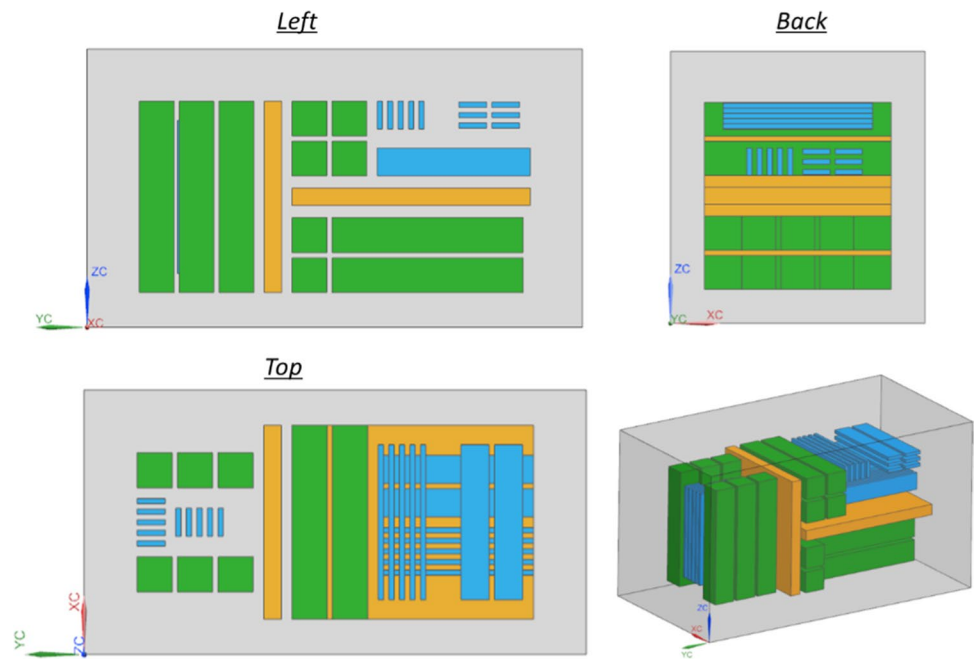


**Table 1** Chemical composition of the filler wire (wt %)

C	Si	Mn	P	S	Cu	Fe
0.088	0.9	1.510	0.012	0.012	0.190	Rest

**Table 2** WAAM process parameters for the blocks

<i>N</i>	WFS, m/min	TS, cm/min	HI, kJ/mm	Inter-pass time, s	Inter-layer time, s	<i>N</i> of passes	<i>N</i> of layers	I, A	U, V
1	2.9	53	0.186	20	905	25	47	123	16.7
2	3.8	38	0.358	23	782	17	36	160	17.7
3	4.6	22	0.762	40	900	11	26	181	19.3

materials could be applied. According to this standard, a rectangular test piece with a thickness of 1.5 mm and width of 2 mm has a total length of test piece equal to 128 mm. Such length of the test piece leads to a significant increase in material usage and deposition time. As a solution, most researchers use rectangular tensile test samples with non-standardized dimensions to characterize the WAAM material. To determine the possible influence of non-standardized test piece dimensions on the ultimate tensile strength, a preliminary study was conducted.

Two kinds of test pieces with non-standardized dimensions were produced using WAAM and compared. Dimensions of the first one were taken from the literature [18], but the length of the gripped ends was increased from 10 to 15 mm to provide proper clamping of the samples (Fig. 7a [18]). In the second test piece, both width and parallel length were increased as shown in Fig. 7b.

Results of the tensile tests (Table 3) show that there is no significant influence of tensile sample dimensions on UTS ( $533 \pm 4.7$  MPa and  $525 \pm 11.5$  MPa, the difference does not exceed 2%). Thus, to determine the influence of welding parameters on the tensile strength of the WAAM parts, tensile specimen dimensions shown in Fig. 7a were used.

Tensile tests for the WAAM blocks were performed at the Belgian Welding Institute using an Instron 8872 machine at room temperature (RT). During the tensile testing, two strain rates were used according to ISO 6892–1:2016. For the determination of the upper yield strength, the strain rate was equal to 0.0035 mm/s (or  $0.00025 \text{ s}^{-1}$ ), after it was increased to 0.067 mm/s ( $0.00478 \text{ s}^{-1}$ ) for the determination of the tensile strength. Elongation after fracture was measured using a HIROX digital microscope KH-8700.



**Fig. 5** Block (HI 0.186 kJ/mm) during deposition

### 2.3 Charpy pendulum impact test piece

In the case of the Charpy pendulum impact test, the amount of energy absorbed depends on the size and geometry of the test piece. Based on this, the standardized test piece dimensions, according to ISO 148–1:2009, were used. Thus, V-notched test pieces with a height and width equal to 10 mm, and a length of 55 mm were produced to determine the amount of absorbed energy. Tests were performed at room temperature.

### 2.4 Vickers hardness testing

A low force Vickers hardness test of HV1 based on EN ISO 6507–1 was performed on the machined surfaces. The specimens were prepared by grinding up to 2400 FEPA scale sandpaper, followed by polishing with 3  $\mu\text{m}$  diamond powder. Tests were implemented on a Shimadzu HMV — 2000 microhardness measurement machine with a 1 kgf load applied for 13 s (according to ISO 6507–1). A standard indenter with an angle of  $136^\circ$  was used. Measurements of indentations were implemented on a HIROX digital microscope KH-8700. Rows of indentations were made according to EN ISO 9015–2 in columnar, coarse grain, and fine grain zones. Recommended distance between indentations  $L=0.5$  mm for HV1 was used.

**Fig. 6** Location of the metallographic and hardness test specimens [22]

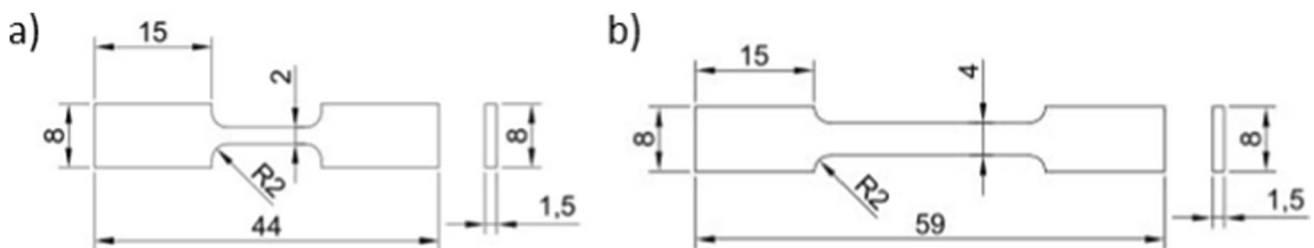
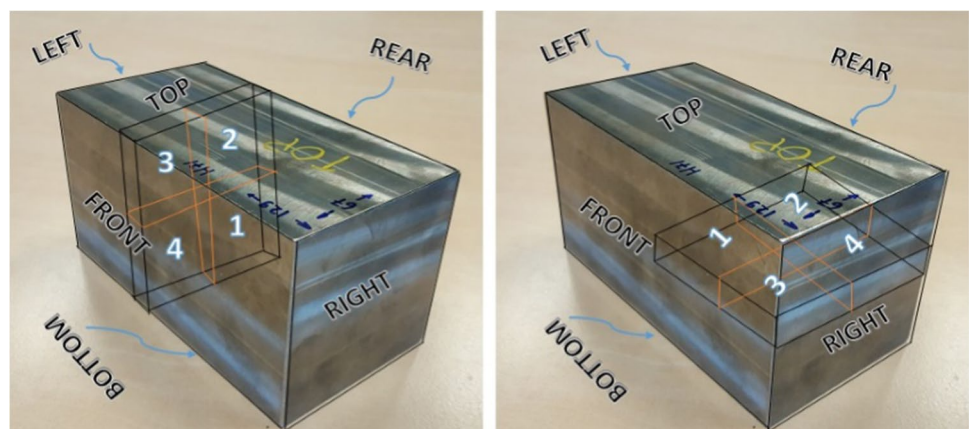


**Fig. 7** Dimensions of non-standardized test pieces **a** taken from the literature, **b** with increased cross-section area and gauge length

**Table 3** Ultimate tensile strength of non-standardized test pieces with different dimensions

<i>N</i>	Cross-section, mm <sup>2</sup>	Maximal load, <i>N</i>	UTS, MPa
1	4×1.5	3223	537
2	4×1.5	3170	528
3	4×1.5	3214	535
4	2×1.5	1619	539
5	2×1.5	1560	519
6	2×1.5	1557	519

### 3 Results

#### 3.1 Microstructure evaluation

The overall microstructure of WAAM material deposited in a multi-pass multilayer way consists of the repetitive pattern of the primary constituent. The primary constituent is a region of one weld bead affected by the adjacent passes, thus containing columnar grain, coarse grain, and fine grain zones. The shape and dimension of the primary constituent are determined by the HI, as shown in Fig. 8. To determine the effect of HI, the microstructure in each region was analysed.

Besides the columnar grain, coarse grain, and fine grain zones, other regions such as the fine grain formed from

previous columnar grain and the intersection of two fine grain zones were detected (Fig. 9). In this study, the influence of the HI on the metallurgical properties of the three main zones (i.e., columnar, coarse grain, and fine grain) is investigated.

The predominant microstructures in the columnar zone are primary ferrite (PF), ferrite side plate (FSP) or Widmanstätten ferrite, and acicular ferrite (AF). It can be seen that the primary ferrite and acicular ferrite are the predominant phases of the WAAM metal. With the increase in HI to 0.358 kJ/mm, cooling time increases (cooling rate, °C/s reduces) and leads to the slightly higher content of primary ferrite and ferrite side plates together with the reduction of the acicular ferrite content (Fig. 10a and b). With a further increase of the HI to 0.762 kJ/mm, the amount of primary ferrite further increases while the amount of Widmanstätten ferrite decreases (Fig. 10c). The morphology of acicular ferrite is different from the previous blocks deposited with lower heat input. They have thicker ferrite plates with blunt tips. This type of acicular ferrite is formed at slower cooling rates and is characterized by larger grain size and is called coarse acicular ferrite (CAF) [19]. The behaviour of these combinations tends to have higher toughness due to the significant reduction of Widmanstätten ferrite and round ends of acicular ferrite needles. Similar microstructural changes with a reduction of cooling rates were observed for usual welds and are shown in the CCT diagram for weld metal in [20, p. 14].

**Fig. 8** Macrostructure of samples deposited with HI **a** 0.186 kJ/mm, **b** 0.358 kJ/mm, **c** 0.762 kJ/mm

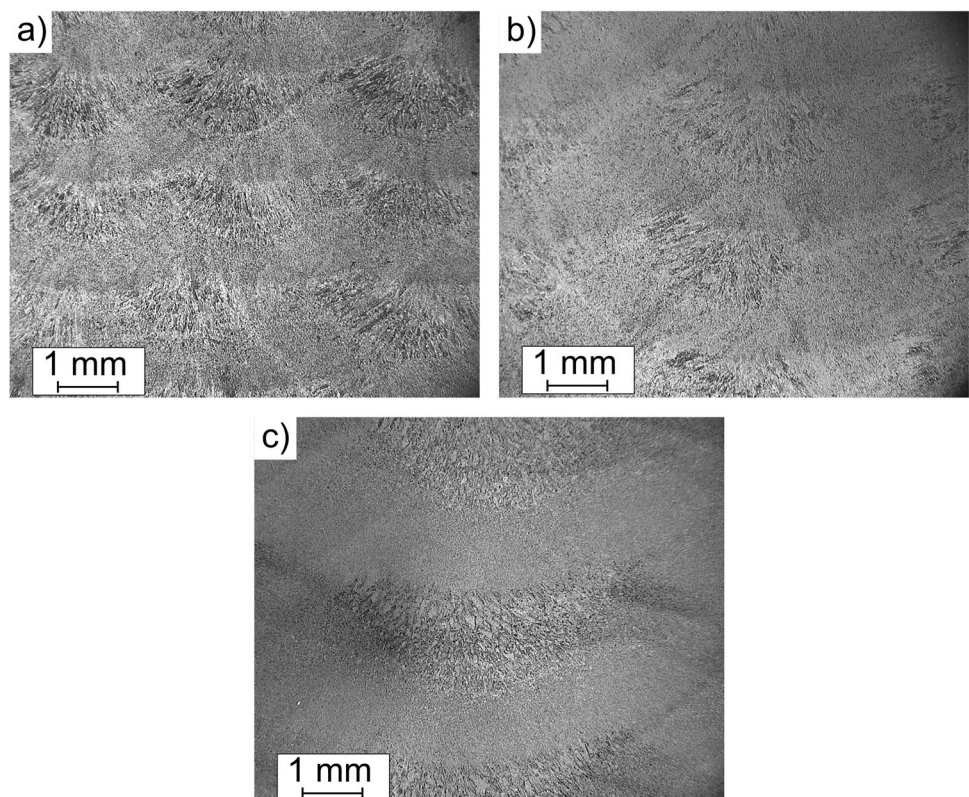


**Fig. 9** Different metallographic regions in WAAM material [22]

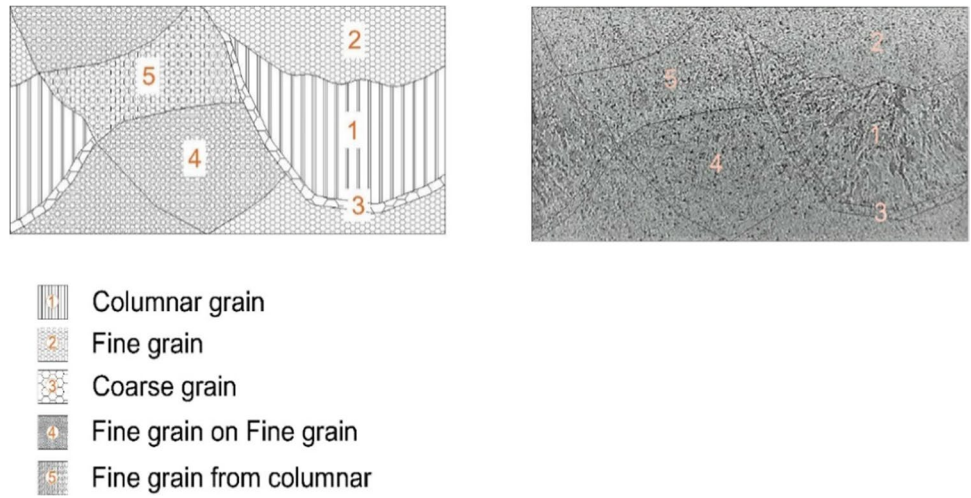
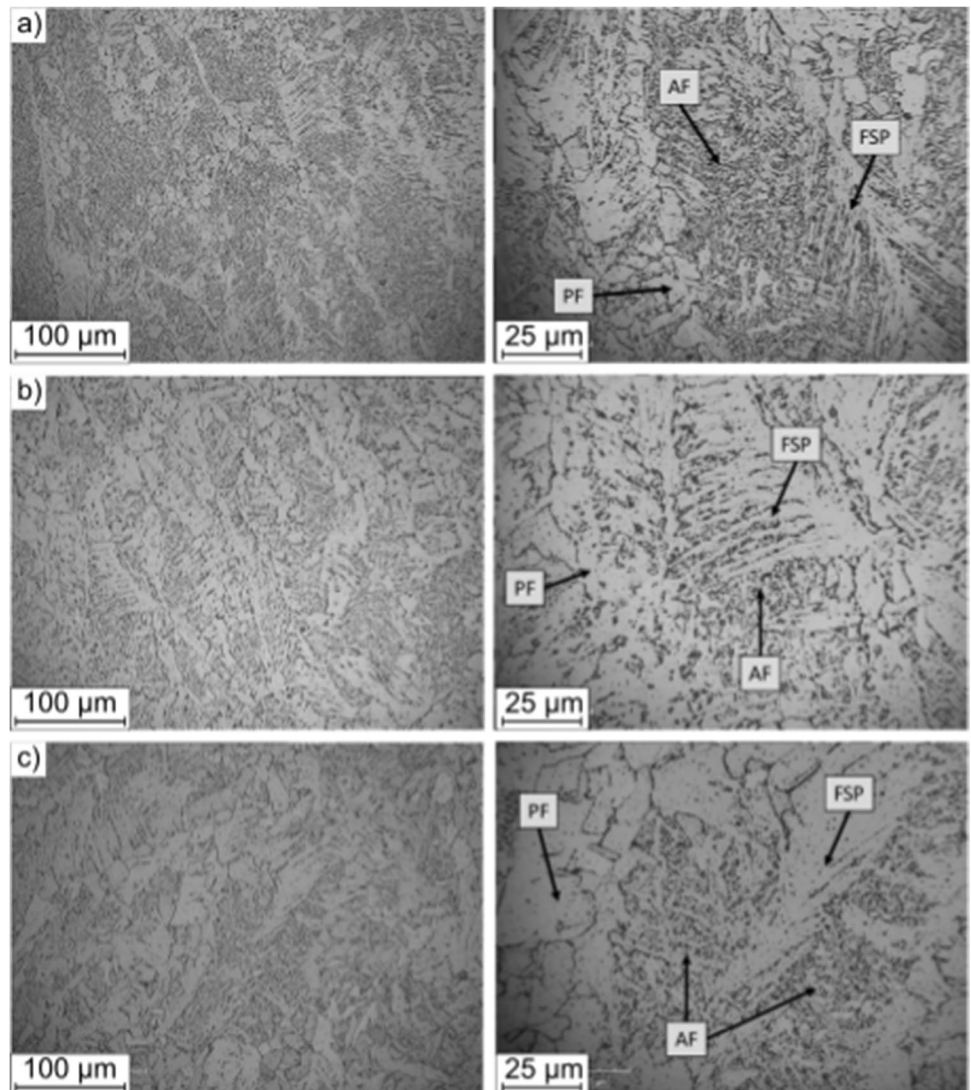


**Fig. 10** Columnar zone micro-structure of sample deposited with **a** HI 0.186 kJ/mm, **b** HI 0.358 kJ/mm, **c** HI 0.762 kJ/mm





The hardness of the acicular ferrite is higher than the primary ferrite ( $2.87 \text{ GPa} > 1.97 \text{ GPa}$  [20] or  $293 \text{ HV} > 201 \text{ HV}$ ). Thus, with the increase of HI, a reduction of hardness in the columnar zone is expected.

The coarse grain HAZ is a narrow region below the fusion line. The width of the coarse grain HAZ depends on the HI and varies from around  $100 \mu\text{m}$  for HI  $0.186 \text{ kJ/mm}$  up to around  $190 \mu\text{m}$  for HI  $0.762 \text{ kJ/mm}$ . The coarse grain region contains coarse primary ferrite, a small amount of acicular ferrite, and bainite (Fig. 11). A similar microstructure was also observed by Shassere et al. [9].

Fine grain HAZ mainly contains refined polygonal ferrite with a small amount of pearlite (black features on triple points of grains). Due to the higher cooling rates, a small amount of bainite may also be present. From Fig. 12, it can be observed that the increase in HI leads to the PF grains coarsening in fine grain HAZ.

From the microstructure characterization, it can be seen that the increase in HI provokes PF grain growth in all three zones. At the same time, coarsening of the PF grains in the coarse grain and fine grain HAZ might result in lower hardness values. According to EN ISO 18265, hardness values are well correlated with tensile strength: for the unalloyed, low-alloy steels and cast-irons tensile strength rises together with hardness. Although the microstructure of the WAAM samples significantly differs from the microstructure of rolled or cast steels, a similar tendency might occur.

### 3.2 Hardness

The rows of indentations were made in the middle of the vertical samples for each block according to ISO 9015–2:2016 (Figs. 13, 14, 15, 16, 17, and 18). Figure 19 shows hardness values in different zones (i.e., columnar, coarse, and fine

**Fig. 11** Coarse grain zone microstructure of sample deposited with **a** HI  $0.186 \text{ kJ/mm}$ , **b** HI  $0.358 \text{ kJ/mm}$ , **c** HI  $0.762 \text{ kJ/mm}$

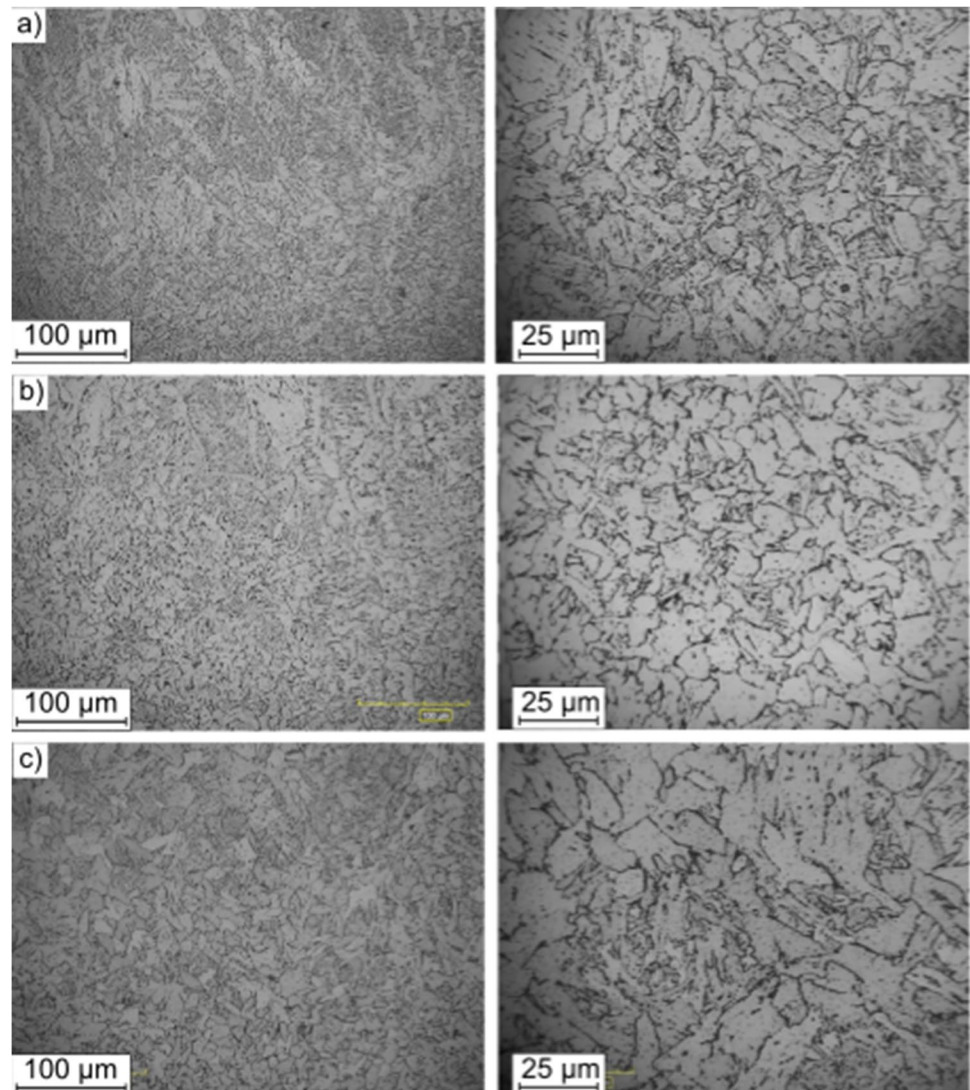
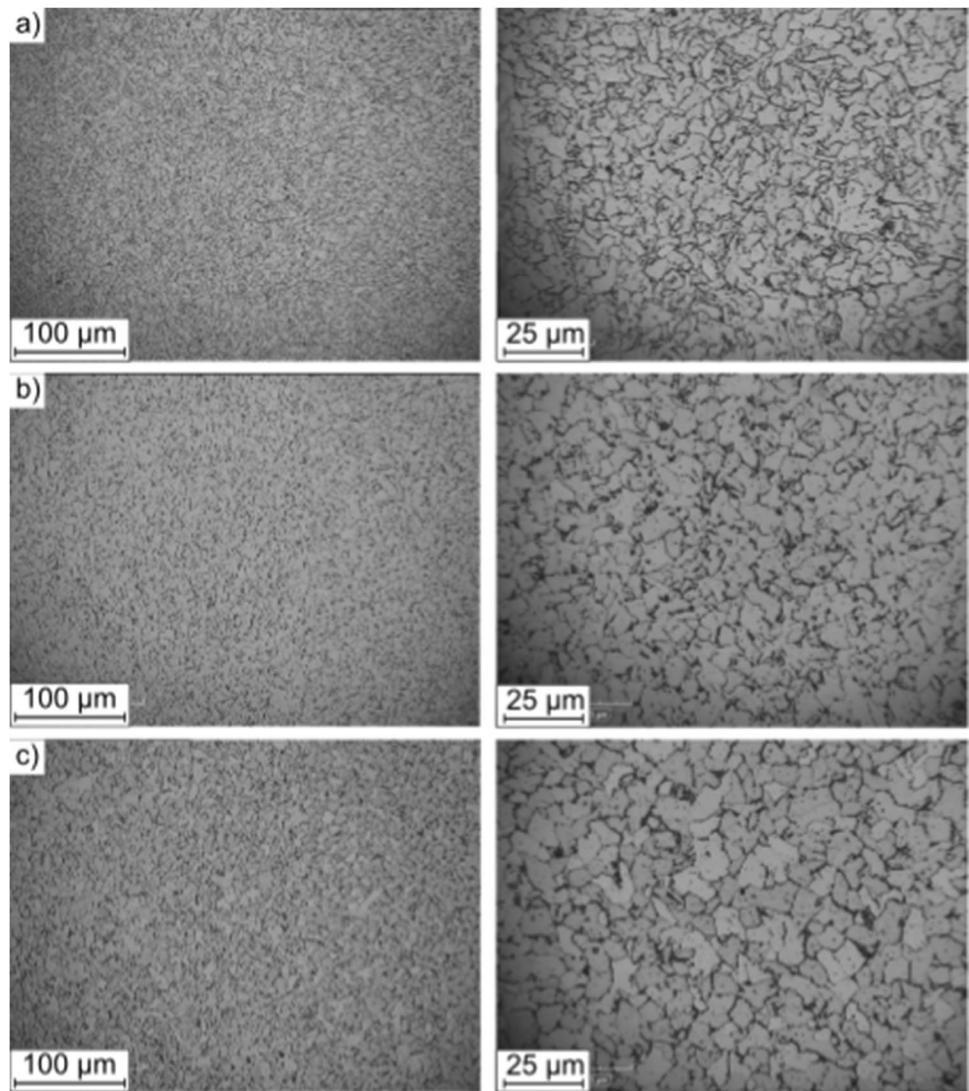


**Fig. 12** Fine grain zone micro-structure of sample deposited with **a** HI 0.186 kJ/mm, **b** HI 0.358 kJ/mm, **c** HI 0.762 kJ/mm



grain zones) depending on the HI. The reduction of HI during WAAM results in higher hardness values in all zones, as was estimated in the previous section.

The highest hardness is observed in the columnar zone and can be explained by the higher percentage of the Widmanstatten ferrite and acicular ferrite. As was stated before,

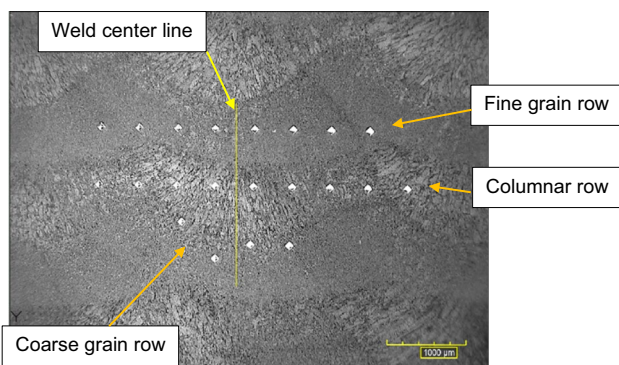


**Fig. 13** Location of indentations in block deposited with HI 0.186 kJ/mm

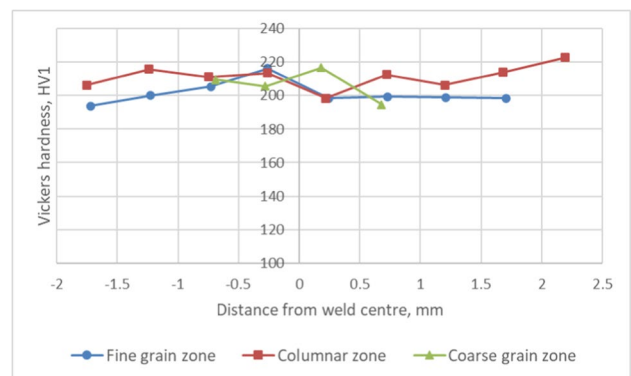


**Fig. 14** Hardness values for rows, HI 0.186 kJ/mm

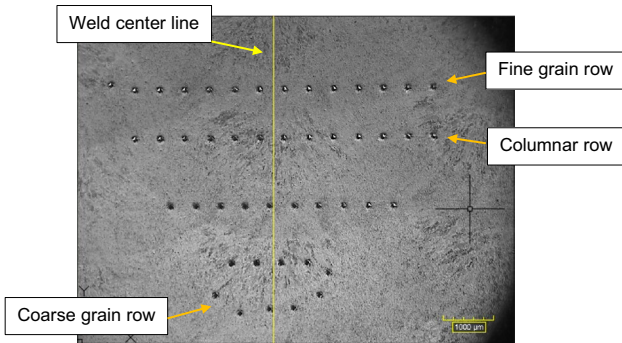


**Fig. 15** Location of indentations in block deposited with HI 0.358 kJ/mm

the hardness of the primary ferrite is lower than the acicular ferrite. Hardness reduces in the coarse grain zone as the dominant phase is a primary ferrite with coarser grains. Nevertheless, the presence of a small amount of acicular ferrite and bainite phases results in the higher hardness of the coarse grain zone compared to the fine grain zone.

### 3.3 Tensile strength

Ultimate tensile strength (Rm) and lower yield strength (ReL) of specimens produced from block 2 (HI 0.358 kJ/mm)

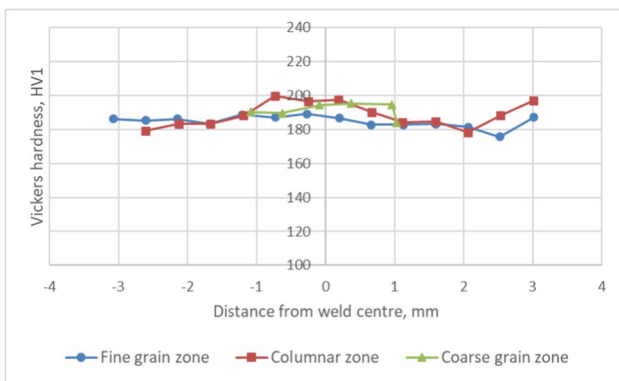


**Fig. 16** Hardness values for rows, HI 0.358 kJ/mm

**Fig. 17** Location of indentations in block deposited with HI 0.762 kJ/mm

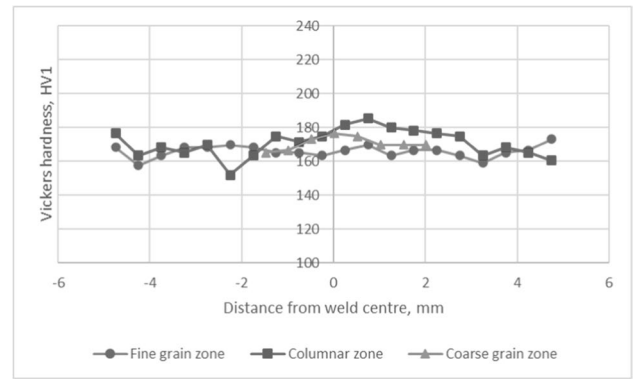
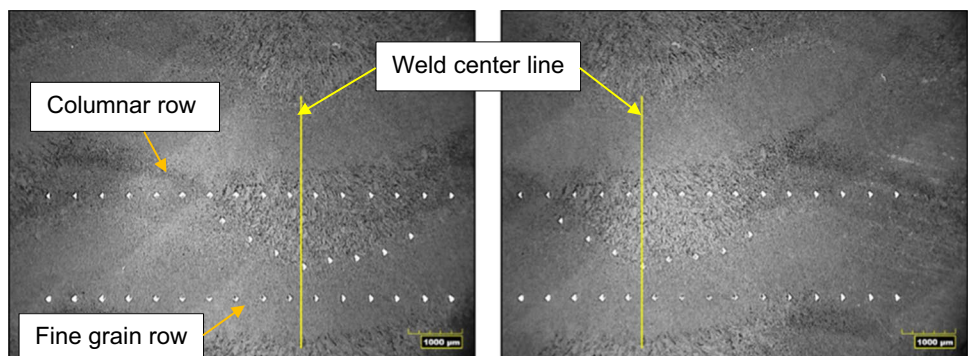


**Fig. 18** Hardness values for rows, HI 0.762 kJ/mm

mm) and block 3 (HI 0.762 kJ/mm) versus the build direction and samples orientation are shown in Figs. 20 and 21 correspondingly.

To evaluate the anisotropy of tensile properties, a one-way analysis of variance (ANOVA) was implemented. Additionally, a test for equal variances was performed to fine-tune the ANOVA. For the 2nd block deposited with HI 0.358 kJ/mm, UTS and lower YS are anisotropic:  $p$ -values equal to 0.007 and 0 correspondingly are lower than significance level  $\alpha=0.05$ . Comparison of means using the Tukey method for UTS (variances are equal) and the Games–Howell method for lower YS (variance of the samples are statistically different) showed that the samples in the vertical direction have significantly higher tensile properties. Nevertheless, it was observed that the orientation of the samples in longitudinal and transversal directions impacts the tensile properties. The effect of the samples' orientation is even more significant for the block deposited with high HI due to the bigger size of the primary constituent. Depending on the sample location, different percentages of coarse grain, fine grain, and columnar microstructures may be present, explaining the scatter in data. The difference of means for the 2nd block between the samples in different directions and orientations does not exceed 3.8% for UTS and 5.1% for lower YS.

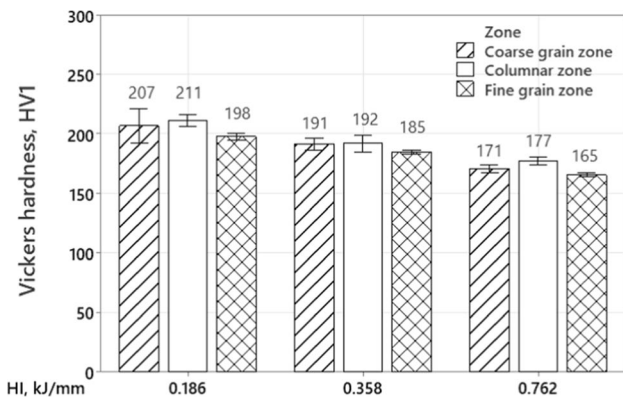


Fig. 19 Hardness of different zones depending on the heat input (HI)

Tensile properties of block 3 deposited with HI 0.762 kJ/mm significantly depend on the orientation of the samples. The ultimate tensile strength for the samples in the longitudinal direction and orientation 2 is significantly higher than the samples in other directions and orientations. The lower yield strength is also anisotropic and depends on the direction and orientation of the samples. The samples in the vertical direction-orientation 1 and longitudinal direction-orientation 1 have lower mean values of lower YS that are significantly different from the other samples. The difference of means for the 3rd block between the samples in different directions and orientations does not exceed 5.6% for UTS and 9.6% for lower YS.

Elongation after fracture is anisotropic for both blocks: *p*-value is equal to 0 for block 2 and 0.025 for block 3. Percentage elongation after fracture is higher for the longitudinal samples (Fig. 22) independently of HI. The difference in elongation after fracture between different directions and orientations is equal to 28.8% and 20.58% for block deposited with HI 0.385 kJ/mm and HI 0.762%, respectively.

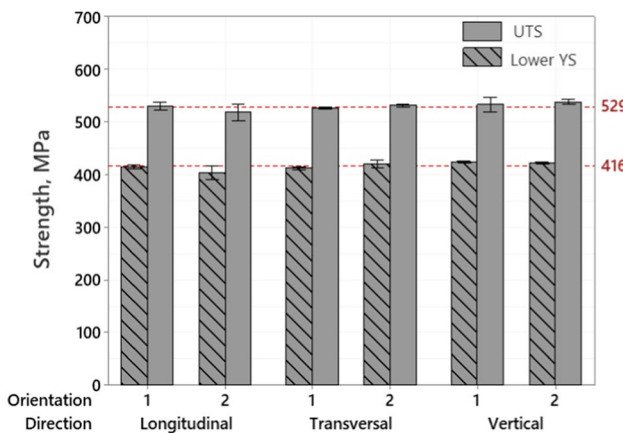


Fig. 20 Ultimate tensile strength (Rm) and lower yield strength (ReL) of deposited specimens (block 2, HI 0.358 kJ/mm) at varying build direction and samples orientation

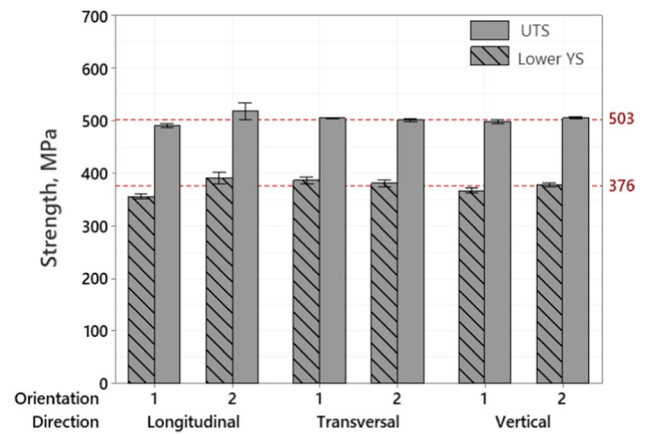


Fig. 21 Ultimate tensile strength (Rm) and lower yield strength (ReL) of deposited specimens (block 3, HI 0.762 kJ/mm) at varying build direction and samples orientation

One can conclude that the tensile properties of WAAM material deposited in a multi-pass multilayer way are anisotropic. The difference in hardness between the columnar and fine grain zones increases with HI resulting in higher anisotropy of the material. For example, the hardness difference between the block deposited with HI 0.358 kJ/mm does not exceed 3.78%, resulting in a difference in UTS of 3.8% and a lower YS of 5.1%. For the block deposited with HI 0.762 kJ/mm, the difference in hardness does not exceed 9.82% resulting in a difference in UTS of 5.6% and 9.6% for lower YS.

An increase in HI shows a negative impact on tensile properties. Block 3 deposited with HI 0.762 kJ/mm has a lower average UTS  $503.34 \pm 10.25$  MPa and YS  $376.56 \pm 13.44$  MPa than the block deposited with HI 0.358 kJ/mm — UTS  $529.97 \pm 8.53$  MPa and YS  $416.89 \pm 7.74$  MPa. Moreover, HI has a more considerable effect on the lower YS (reduction by 10.7%) than on UTS

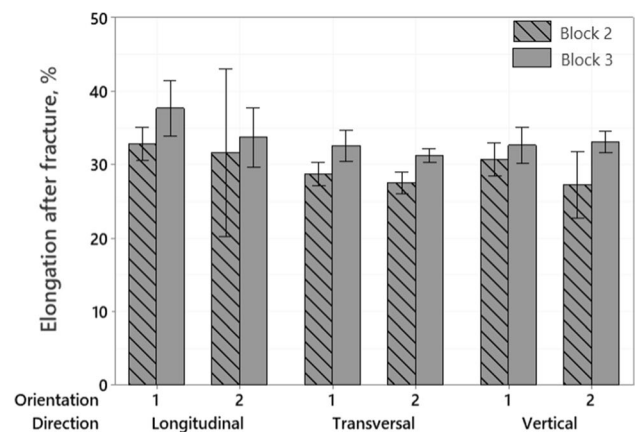


Fig. 22 Percentage elongation after fracture at varying build direction and sample orientation

(reduction by 5.3%). Nevertheless, the rise of HI has a positive impact on elongation after fracture (higher by 12%). With the increase in HI, cooling time also increases, even if the interpass temperature is the same. An increase in cooling time provokes the growth of primary ferrite grains, the reduction of Widmanstatten ferrite amount, and coarsening of the acicular ferrite. This leads to a decrease in the material's hardness and tensile strength.

### 3.4 Charpy impact toughness

One-way ANOVA was used to determine whether the difference between means of samples with different directions and orientations is statistically significant. For the block deposited with HI 0.358 kJ/mm, the direction and orientation of the samples have a significant effect on the impact toughness ( $p$ -value equal to 0). Vertical samples are characterized by the lowest toughness values, which do not depend on the sample orientation. The toughness of the transversal and longitudinal samples depends on the orientation of the test specimens (Fig. 23). This phenomenon can be explained by the location of the notch. Todinov et al. [21] stated that “the type of microstructure in which the notch root is located has a crucial role in the distribution of impact energy values.” It was shown that the samples with the notch located in the reheated zone along the weld direction have higher impact toughness than the samples with the notch located in the columnar zone (centre of the weld bead).

With the increase in HI, the toughness value becomes more uniform along different directions (Fig. 24). For the block deposited with a higher HI (0.762 kJ/mm), the orientation of the notch does not impact the toughness of the material ( $p$ -value equal to 0.456). The direction is also not statistically significant ( $p$ -value equal to 0.651). Thus, it can be concluded that the block produced with high HI has isotropic impact toughness.

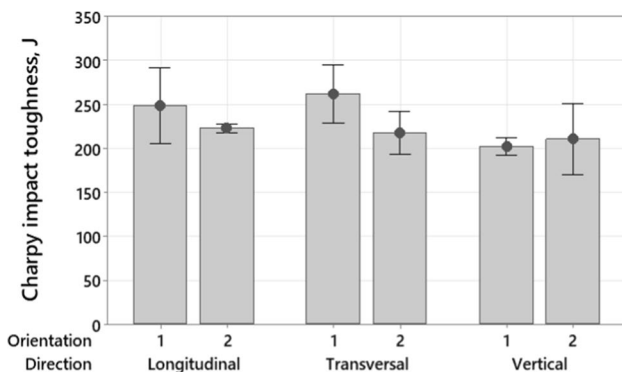


**Fig. 23** Impact toughness of the block deposited with HI 0.358 kJ/mm measured at RT

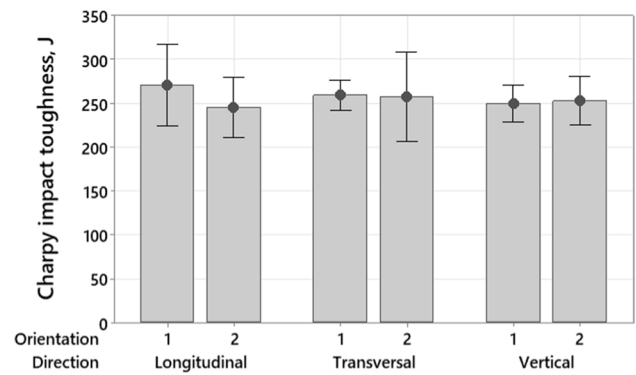


**Fig. 24** Impact toughness of the block deposited with HI 0.762 kJ/mm measured at RT

HI also significantly affects the average impact toughness of the material ( $p$ -value equals 0). With the increase of HI, the average value of impact toughness rises from 227 to 255 J at RT.

## 4 Discussion

The mechanical properties of WAAM components deposited in a multi-pass multilayer way significantly depend on HI and cooling time from 800 to 500 °C during the deposition process. An increase in cooling time provokes the growth of primary ferrite, reduction of the amount of Widmanstatten ferrite, and coarsening of the acicular ferrite. Such changes in microstructure result in lower hardness and tensile strength of the material. As the WAAM material is represented by the repetitive pattern of the primary constituent, which contains three main regions with different microstructures, the tensile properties of the material are anisotropic and depend on the samples' direction and orientation. The impact toughness of the material depends on HI as well. As such, an increase in HI leads to isotropic properties with higher toughness values.

To select the welding wire for the production of a functional component using WAAM, it is important to compare the properties of the WAAM material with the properties specified in the welding wire certificate and corresponding standard and the properties of steels produced in a conventional way. Copper coated solid filler wire LASTIFIL 20 from LASTEK was used to determine the mechanical properties of WAAM parts. All the wire rolls belong to one batch. Properties of the wire and weld deposits correspond to the requirements of EN ISO 14341-A G 42 4 M21 3Si1. Material properties of the conventional hot-rolled steel, filler wire material, and WAAM material are given in Table 4.

Tensile properties of the WAAM material are significantly lower than the properties of the welding wire specified in the

**Table 4** Mechanical properties of structural steels, filler wire, and WAAM material

Material	Min ReH, Mpa	Min ReL, Mpa	Min Rm, MPa	Max Rm, MPa	Min A, %	Min impact toughness, J
S235JR <sup>1</sup>	215	-	360	510	24	27 at RT
S275JR <sup>1</sup>	245	-	410	560	21	27 at RT
S355JR <sup>1</sup>	325	-	470	630	20	27 at RT
Filler wire (G 42 4 M21 3Si1) according to the standard <sup>2</sup>	-	420	500	640	20	≥ 47 J at -40 °C
Filler wire (G 42 4 M21 3Si1) according to the inspection certificate <sup>3</sup>	-	465	583	-	-	≥ 47 J at -40 °C
WAAM 0.358 <sup>4</sup>	397	392	502	549	23	196 at RT
WAAM 0.762 <sup>4</sup>	356	349	487	535	28	230 at RT

where ReH — upper yield strength, ReL — lower yield strength, Rm — tensile strength, A — percentage elongation after fracture

<sup>1</sup>Properties of base material — according to EN ISO 10025–2: Hot-rolled products of structural steels — part 2: technical delivery conditions for non-alloy structural steels for nominal thickness 75 mm

<sup>2</sup>ISO 14341:2010, Welding consumables — wire electrodes and weld deposits for gas shielded metal arc welding of non alloy and fine grain steels — classification

<sup>3</sup>Inspection certificate EN 3.1 (EN 10,204) for welding wire provided by Lastek Belgium NV

<sup>4</sup>The minimum values obtained from the WAAM material testing

inspection certificate (583 MPa). However, the UTS of the WAAM blocks corresponds to the EN ISO 14341 standard (500–640 MPa). On the contrary, the lower YS is lower than the value specified in both the wire certificate (465 MPa) and the standard (420 MPa). This is due to the difference in heat transfer between the blocks produced by WAAM and standard butt joint multi-pass welding. In traditional multi-pass welding, heat dissipates through 3D cooling to the base metal (conduction) and by radiation and convection to the environment. Heat loss by conduction is the most effective resulting in higher cooling rates, higher hardness values, and thus tensile properties. In the case of WAAM, heat is mainly dissipated through convection and radiation. With the increase of the build height, heat accumulation occurs, leading to lower cooling rates. To select the right welding wire for WAAM and achieve the required material properties, a comparison of the mechanical properties was made (Table 5). For comparison, the minimum values obtained from the WAAM material testing were taken. Based on these values, the following estimation can be applied:

**Table 5** Comparison of the filler wire and WAAM material mechanical properties

	WAAM/filler metal ratio (%)
Yield strength ReH, MPa	-
Yield strength ReL, MPa	88
Tensile strength Rm min, MPa	95
Elongation after fracture A, %	115

- The lower YS (ReL) of the WAAM material ≈ 88% of the lower YS specified in the standard for welding consumables ISO 14341.
- Minimum UTS (Rm) of the WAAM material ≈ 95% of the minimum UTS specified in the standard for welding consumables ISO 14341
- Elongation after fracture (A) of the WAAM material ≈ 115% of the elongation after fracture specified in the standard for welding consumables ISO 14341

For design purposes, the WAAM material's properties should be compared to the properties of steel products. The comparison showed that the properties of the WAAM material exceed the properties of S235JR, S275JR, and S355JR (Table 6). Nevertheless, certain precautions should be taken when the S235JR steel is replaced with WAAM

**Table 6** Comparison of the hot-rolled steel and WAAM material mechanical properties

Material	WAAM/hot-rolled metal ratio (%)				
	ReH, Mpa	Rm min, MPa	Rm max, MPa	A, %	Impact toughness, J
S235JR*	166%	135%	105%	124%	725%
S275JR*	145%	118%	95%	141%	725%
S355JR*	109%	103%	85%	149%	725%

\*Properties of base material — according to EN ISO 10025–2: Hot-rolled products of structural steels — part 2: technical delivery conditions for non-alloy structural steels for nominal thickness 75 mm

material as the maximum UTS of the WAAM exceeds the maximum UTS of S235JR specified in EN ISO 10025–2 standard.

A similar approach can be used for cast and forged steels. Still, mechanical testing should be implemented on the prototypes as the properties of the WAAM material are highly dependent on the design of the part, deposition strategy used, WAAM process parameters, welding power source characteristics, PWHT, etc.

## 5 Conclusion

The impact of the welding heat input on the microstructure and mechanical properties of the WAAM components produced in a multi-pass multilayer way has been determined. The microstructure of the solid WAAM parts consists of the repetitive pattern of the primary constituent, which contains columnar, coarse grain, and fine grain zones. The increase in HI provokes PF grain growth in all zones of the primary constituent. In the columnar zone, the amount of FSP first increases when HI rises from 0.186 to 0.358 kJ/mm and further reduces when HI is 0.762 kJ/mm. Additionally, the increase in HI causes a reduction of the acicular ferrite microstructure and its coarsening. Such changes in microstructure caused by the increase in HI result in lower material hardness and reduced tensile strength. Nevertheless, the rise of HI has a positive impact on elongation after fracture. The tensile properties of the material are anisotropic. The location and orientation of the specimen define the percentage of the columnar zone, coarse grain, and fine grain HAZ, leading to scatter in tensile properties. The isotropy of the impact toughness depends on HI. The increase in HI from 0.358 to 0.762 kJ/mm leads to more isotropic impact toughness of the material and an increase in the amount of absorbed energy.

The properties of the WAAM material were compared to properties specified in: (1) the welding wire certificate and (2) the EN ISO 14341 standard, (3) properties of hot-rolled structural steels. The comparison showed that the G 42 4 M21 3Si1 (EN ISO 14341-A) wire can be used to produce functional components using WAAM as an alternative for conventional subtractive manufacturing of parts from S275JR and S355JR structural steels taking static loads and impact loads. Additionally, the reference for the filler wire selection was provided based on the required mechanical properties of the WAAM component.

However, mechanical testing should be implemented on the prototypes as the properties of the WAAM material are highly dependent on the design of the part, deposition strategy used, WAAM process parameters, welding power source characteristics, PWHT, etc.

**Acknowledgements** The authors would like to thank the Machine Tool Technologies Research Foundation (MTTRF) for supporting CNC Machining Centers to KU Leuven. The research has also been made possible through the financial support of the Flanders Agency for Innovation & Entrepreneurship (VLAIO) and through the projects VIS “3d printen via (standard) lasrobot: wire and arc additive manufacturing” and TETRA-CORNET “Advanced processing of additively manufactured parts.”

**Author contribution** NC: conceptualization, methodology, investigation, validation, formal analysis, writing — original draft, visualization; FM: formal analysis, writing — original draft, visualization; BL: writing — review and editing, supervision, funding acquisition; PVR: writing — review and editing, supervision, funding acquisition.

## Declarations

**Competing interests** The authors declare no competing interests.

## References

- Davies R (2015) Industry 4.0. Digitalisation for productivity and growth. Eur Parliam Res Serv no. September 10
- Coykendall J, Cotteleer M, Holdowsky L, Mahto M (2014) 3D opportunity in aerospace and defense. Deloitte University Press 1–28
- Williams SW, Martina F, Addison AC, Ding J, Pardal G, Colegrove P (2016) Wire + arc additive manufacturing. Mater Sci Technol 32(7):641–647. <https://doi.org/10.1179/1743284715Y.0000000073>
- Wu B, Pan Z, Ding D, Cuiuri D, Li H (2018) Effects of heat accumulation on microstructure and mechanical properties of Ti6Al4V alloy deposited by wire arc additive manufacturing. Addit Manuf 23(August):151–160. <https://doi.org/10.1016/j.addma.2018.08.004>
- Zhang X, Martina F, Ding J, Wang X, Williams SW (2017) Fracture toughness and fatigue crack growth rate properties in wire + arc additive manufactured Ti-6Al-4V. Fatigue Fract Eng Mater Struct 40(5):790–803. <https://doi.org/10.1111/ffe.12547>
- Ge J, Lin J, Chen Y, Lei Y, Fu H (2018) Characterization of wire arc additive manufacturing 2Cr13 part: process stability, microstructural evolution, and tensile properties. J Alloy Compd 748:911–921. <https://doi.org/10.1016/j.jallcom.2018.03.222>
- Zhang C, Li Y, Gao M, Zeng X (2018) Wire arc additive manufacturing of Al-6Mg alloy using variable polarity cold metal transfer arc as power source. Mater Sci Eng A 711(November 2017):415–423. <https://doi.org/10.1016/j.msea.2017.11.084>
- Song HY, Evans GM, Babu SS (2014) Effect of microstructural heterogeneities on scatter of toughness in multi-pass weld metal of C-Mn steels. Sci Technol Weld Joining 19(5):376–384. <https://doi.org/10.1179/1362171814y.0000000194>
- Shassere B, Nycz A, Noakes MW, Masuo C, Sridharan N (2019) Correlation of microstructure and mechanical properties of metal big area additive manufacturing. Appl Sci (Switzerland) 9(4) <https://doi.org/10.3390/app9040787>
- Liberini M et al (2017) Selection of optimal process parameters for wire arc additive manufacturing. Procedia CIRP 62:470–474. <https://doi.org/10.1016/j.procir.2016.06.124>
- Rodrigues TA, Duarte V, Avila JA, Santos TG, Miranda RM, Oliveira JP (2019) Wire and arc additive manufacturing of HSLA steel: effect of thermal cycles on microstructure and mechanical

- properties. *Addit Manuf* 27(February):440–450. <https://doi.org/10.1016/j.addma.2019.03.029>
12. Haden CV, Zeng G, Carter FM, Ruhl C, Krick BA, Harlow DG (2017) Wire and arc additive manufactured steel: tensile and wear properties. *Addit Manuf* 16:115–123. <https://doi.org/10.1016/j.addma.2017.05.010>
  13. Lu X, Zhou YF, Xing XL, Shao LY, Yang QX, Gao SY (2017) Open-source wire and arc additive manufacturing system: formability, microstructures, and mechanical properties. *Int J Adv Manuf Technol* 93(5–8):2145–2154. <https://doi.org/10.1007/s00170-017-0636-z>
  14. Waqas A, Xiansheng Q, Jiangtao X, Chaoran Y, Fan L (2018) Impact toughness of components made by GMAW based additive manufacturing. *Procedia Struct Integr* 13:2065–2070. <https://doi.org/10.1016/j.prostr.2018.12.207>
  15. Sridharan N, Noakes MW, Nycz A, Love LJ, Dehoff RR, Babu SS (2018) On the toughness scatter in low alloy C-Mn steel samples fabricated using wire arc additive manufacturing. *Mater Sci Eng A* 713(November 2017):18–27. <https://doi.org/10.1016/j.msea.2017.11.101>
  16. Fu J et al (2017) Effect of tool-path on morphology and mechanical properties of Ti-6Al-4V fabricated by wire and arc additive manufacturing. *MATEC Web Conf* 128:05009. <https://doi.org/10.1051/mateconf/201712805009>
  17. Song YA, Park S, Chae SW (2005) 3D welding and milling: part II — optimization of the 3D welding process using an experimental design approach. *Int J Mach Tools Manuf* 45(9):1063–1069. <https://doi.org/10.1016/j.ijmactools.2004.11.022>
  18. Ma Y, Cuiuri D, Hoye N, Li H, Pan Z (2015) The effect of location on the microstructure and mechanical properties of titanium aluminides produced by additive layer manufacturing using in-situ alloying and gas tungsten arc welding. *Mater Sci Eng A* 631:230–240. <https://doi.org/10.1016/j.msea.2015.02.051>
  19. Zhang Z, Ferrar RA (1995) An atlas of continuous cooling transformation (CCT) diagrams applicable to low carbon low alloy weld metals, 638. Institute of Materials
  20. Liu K, Wang D, Deng C, Gong B, Wu S (2020) Improved microstructure heterogeneity and low-temperature fracture toughness of C-Mn weld metal through post weld heat treatment. *Mater Sci Eng A* 770(August 2019):138541. <https://doi.org/10.1016/j.msea.2019.138541>
  21. Todinov MT, Novovic M, Bowen P, Knott JF (2000) Modelling the impact energy in the ductile/brittle transition region of C-Mn multi-run welds. *Mater Sci Eng A* 287(1):116–124. [https://doi.org/10.1016/S0921-5093\(00\)00824-8](https://doi.org/10.1016/S0921-5093(00)00824-8)
  22. Marefat F (2020) Determination of process parameters' influence on mechanical properties and microstructure of low-alloyed low carbon steel produced by wire and arc additive manufacturing. KU Leuven, Faculteit Industriële Ingenieurswetenschappen
- Publisher's note** Springer Nature remains neutral with regard to jurisdictional claims in published maps and institutional affiliations.
- Springer Nature or its licensor (e.g. a society or other partner) holds exclusive rights to this article under a publishing agreement with the author(s) or other rightsholder(s); author self-archiving of the accepted manuscript version of this article is solely governed by the terms of such publishing agreement and applicable law.